Computer Assisted Mechanics and Engineering Sciences, **13**: 305–322, 2006.

Effective elastic properties of periodic fibrous composites. Limit cases. Applications to porous and nonlinear materials

Julián Bravo-Castillero, Raúl Guinovart-Díaz,
Reinaldo Rodríguez-Ramos
Facultad de Matemática y Computación
Universidad de La Habana
San Lázaro y L, Vedado, Habana 4, CP–10400, Cuba

Federico J. Sabina
Instituto de Investigaciones en Matemáticas Aplicadas y en Sistemas
Universidad Nacional Autónoma de México, Apartado Postal 20–726
Delegación de Alvaro Obregón, 01000 México, D.F., México

Oscar C. Valdiviezo-Mijangos
*Posgrado en Ciencias de la Tierra, Ciudad Universitaria, 04510 México, D.F., México**
**Present address: Instituto Mexicano del Petróleo*
Eje Central Lázaro Cárdenas 152, San Bartolo Atepehuacan
Delegación Gustavo A. Madero, 07730 México, D.F., México

José Claudio Sabina-de-Lis
Departamento de Análisis Matemático, Universidad de La Laguna
E-38271 La Laguna, Tenerife, España

(Received October 18, 2004)

The goal of this contribution is to provide, based on the asymptotic homogenization method, helpful exact formulae to compute the overall stiffnesses and engineering moduli of a transversely isotropic two-phase fibre reinforced composite with isotropic constituents. Comparison of the exact solution with known bounds is shown. In certain cases a bound is very close to the exact solution over a large interval. The bound then could be used as a good approximation to the exact solution. The exact formulae explicitly display Avellaneda and Swart's microestructural parameters, which have a physical meaning, and provide formulae for them. Hill's universal relations follow from the formulae. Limiting cases of rigid and empty fibers are included. An application of these results to improve bounds for the effective energy density of nonlinear dielectric fibrous composites is shown. Another application is related to bone poroelasticity.

Keywords: fibers, mechanical properties, microstructure, anisotropy, elastic properties

1. Introduction

This paper is concerned with the problem of finding effective properties of a two-phase fibre-reinforced composite whose constituents are isotropic elastic. The fibres are arranged in an hexagonal array. The fibre cross-section is circular. Recently, [6] and [14] derived exact closed-formulae for the effective coefficients of a more general case of this composite, with the individual phases possesing

the elastic and piezoelectric transversely isotropic symmetry, by applying the asymptotic homogenization method. Such derivation is based on the solution of the corresponding local problems by using the potential methods of a complex variable and the properties of doubly periodic Weierstrass and related functions, as in [10, 11, 13, 15], for the case of square symmetry and isotropic constituents. The basis of all these works are in [5]. The homogenization method is well-known. References to text books and many applications can be found in [6]. Here exact closed-form formulae are provided directly from the formulation of [6] in a way that is suitable for a relatively easy computation. This specialisation also allows the obtention of explicit closed-form formulae for the limiting cases of empty and rigid fibers. The importance of these results to obtain improved bounds for nonlinear fibrous composites based on the variational formulation of [18, 19] is illustrated in two examples. Another application related to bone poroelasticity is given.

Section 2 starts with the statement of the problem, introducing the effective stiffnesses and engineering constants. Section 3 gives the exact closed-form formulae for the overall properties of the two-phase composite with isotropic constituents and hexagonal symmetry. Analogous formulae are also given for the two limiting cases of empty or rigid fibers, the derivation of which are included in Appendices C-E. In Sec. 4 several examples are shown; comparison among the exact solution and known bounds is shown. Two examples of applications for bounding the effective energy density of nonlinear dielectric composites is also dealt. Note that the problem of dielectrics is mathematically equivalent to those of thermal and electric conductivity, magnetic permeabilities or diffusion coefficients; thus, the results given in this paper apply to the previously mentioned physical properties as well. Some final remarks are contained in Sec. 5. Appendix A defines parameters which appear in the exact formulae. Appendix B defines vectors, matrices and series relevant to the formulae.

2. Statement of the problem

A two-phase fibre reinforced composite is studied here in which the properties of the constituents are homogeneous and elastic. The Ox_3 direction is the axis of symmetry. The fibers have a circular cross-section and they are periodically distributed without overlapping in directions parallel to the Ox_1 axes and the lines with slope at an angle $\pi/3$, corresponding to hexagonal symmetry (Fig. 1). Thus, the composite effective properties are transversely isotropic. The non-zero terms of the stress-strain constitutive relation may be written as a function of five independent parameters k^*, l^*, n^*, p^* and m^* as follows:

$$\begin{aligned}
\frac{1}{2}(\sigma_{11}+\sigma_{22}) &= k^*(\epsilon_{11}+\epsilon_{22})+l^*\epsilon_{33},\\
\sigma_{33} &= l^*(\epsilon_{11}+\epsilon_{22})+n^*\epsilon_{33},\\
\sigma_{11}-\sigma_{22} &= 2m^*(\epsilon_{11}-\epsilon_{22}),\\
\sigma_{32} &= 2p^*\epsilon_{32},\\
\sigma_{31} &= 2p^*\epsilon_{31},\\
\sigma_{12} &= 2m^*\epsilon_{12},
\end{aligned} \tag{1}$$

where σ_{ij} are the components of the stress tensor, the indices i, j range from 1 to 3, the components of the strain tensor ϵ_{ij} are defined by

$$\epsilon_{ij} = \frac{1}{2}\left(\frac{\partial u_i}{\partial x_j}+\frac{\partial u_j}{\partial x_i}\right), \tag{2}$$

here the components of the displacement vector are u_i; k^* is the plane-strain bulk modulus for lateral dilatation without longitudinal extension; l^* is the associated cross-modulus; n^* is the modulus for longitudinal uniaxial extension; p^* and m^* are, the rigidity moduli for shearing in the

longitudinal and in any transverse directions, respectively. The engineering constants are related to these moduli through

$$
\begin{aligned}
&E_a^* = n^* - l^{*2}/k^* = n^* - 4k^*(\nu_a^*)^2,\\
&\nu_a^* = l^*/2k^*,\\
&E_t^* = 4k^*m^*/(k^* + n^*m^*/E_a^*) = 2(1+\nu_t^*)m^*,\\
&\nu_t^* = (k^* - n^*m^*/E_a^*)/(k^* + n^*m^*/E_a^*),
\end{aligned}
\tag{3}
$$

where the subindices a and t refer to an axial or transverse property, respectively. The Young moduli are denoted by E_a^*, E_t^* and the Poisson ratio by ν_a^* and ν_t^*. Also subindices 1 and 2 correspond to a quantity related to the matrix and by the fiber, in that order. Bulk and ridigity moduli of the phases are defined by K and μ, respectively. The volume fraction per unit length occupied by the matrix is V_1 and by the fiber $V_2 = \pi R^2/\sin(\pi/3)$ so that $V_1 + V_2 = 1$. The Voigt or arithmetic mean of a certain property are given below as

$$
\begin{aligned}
&K_v = K_1V_1 + K_2V_2,\\
&\mu_v = \mu_1V_1 + \mu_2V_2.
\end{aligned}
\tag{4}
$$

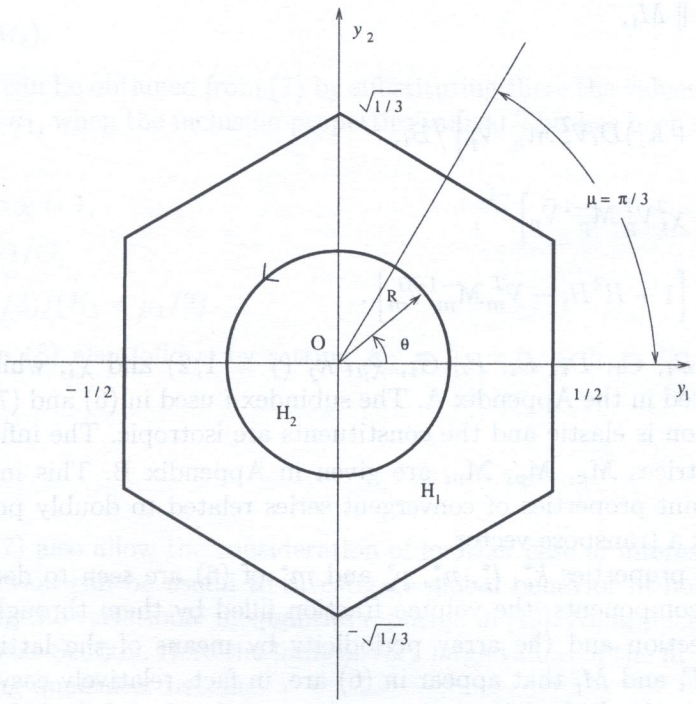

Fig. 1. Hexagonal unit cell

The contrast of a property across the matrix-fiber interface is determined by means of the double bar notation as

$$
\begin{aligned}
&\| K \| = K_1 - K_2,\\
&\| \mu \| = \mu_1 - \mu_2.
\end{aligned}
\tag{5}
$$

The main purposes of this paper is to produce helpful exact formulae to compute overall stiffnesses and engineering moduli; including limit cases for empty and rigid fibers; and to show their importance for obtaining improved bounds for nonlinear fibrous composites.

3. Two-phase elastic composite

In a recent study, [6] analysed a similar fiber-reinforced composite with the same geometry except that both elastic constituents have transversely isotropic properties. The composite overall parameters are obtained by means of the asymptotic homogenization method, the application of the Kolosov–Muskhelishvili complex potentials and properties of doubly periodic functions. The final formulae (Eqs. (3.15), (3.16), (3.33) and (3.34) in [6]) can be used for isotropic components as well. The transversely isotropic material parameters, k, l, n, p and m, are related to the isotropic material parameters by $k = K + \mu/3$, $l = K - 2\mu/3$, $n = K + 4\mu/3$, $p = m = \mu$ with $K = E/[3(1-2\nu)]$ and $\mu = E/[2(1+\nu)]$ being the conventional bulk modulus and shear modulus, respectively. Although the constituents are isotropic the overall properties of the hexagonal array have 6mm symmetry. The substitution of these produces the formulae

$$
\begin{aligned}
k_i^* &= K_v + \mu_v/3 - V_2 \parallel K + \mu/3 \parallel^2 K_i/\mu_1, \\
l_i^* &= K_v - 2\mu_v/3 - V_2 \parallel K + \mu/3 \parallel\!\!\parallel K - 2\mu/3 \parallel K_i/\mu_1, \\
n_i^* &= K_v + 4\mu_v/3 - V_2 \parallel K - 2\mu/3 \parallel^2 K_i/\mu_1, \\
p_i^* &= \mu_1 \left[1 - 2V_2 \parallel \mu \parallel P_i/(\mu_1 + \mu_2)\right], \\
m_i^* &= \mu_1 - V_2 \parallel \mu \parallel M_i,
\end{aligned}
\tag{6}
$$

where

$$
\begin{aligned}
K_i &= D_i \left[V_1 + (1+\kappa_1) D_i \mathcal{V}_p^T \mathcal{M}_k^{-1} \tilde{\mathcal{V}}_p\right] / B_i, \\
P_i &= \left[1 + \chi_i V_2 - \chi_i^2 \mathcal{V}_p^T \mathcal{M}_p^{-1} \tilde{\mathcal{V}}_p\right]^{-1}, \\
M_i &= (1+\kappa_1) E_i / \left[1 + R^2 H_i - \mathcal{V}_m^T \mathcal{M}_m^{-1} \tilde{\mathcal{V}}_m^T\right].
\end{aligned}
\tag{7}
$$

The parameters A_i, B_i, C_i, D_i, E_i, F_i, G_i, χ_μ, κ_j $(j = 1, 2)$ and χ_i, which appear in (7) and (B2)–(B4), are collected in the Appendix A. The subindex i used in (6) and (7) refers to the general case when the inclusion is elastic and the constituents are isotropic. The infinite order vectors $\mathcal{V}_p$, $\tilde{\mathcal{V}}_p$, $\mathcal{V}_m$, $\tilde{\mathcal{V}}_m$ and matrices $\mathcal{M}_k$, $\mathcal{M}_p$, $\mathcal{M}_m$ are given in Appendix B. This includes the parameter H_i as well as important properties of convergent series related to doubly periodic functions. The superindex T denotes a transpose vector.

The above overall properties k_i^*, l_i^*, n_i^*, p_i^* and m_i^* of (6) are seen to depend on the isotropic caracteristics of the components, the volume fraction filled by them through the radius R of the fiber circular cross-section and the array periodicity by means of the lattice sums S_k, T_k. The three quantities K_i, P_i and M_i that appear in (6) are, in fact, relatively easy to compute. Enough accurate results are obtained after truncation to the second order of the infinite order vectors and matrices. The powers of R, a number less than one-half appear frequently as can be seen in (B1)–(B3). The series involved also converge very quickly thus simplifying considerable the computational effort.

The structure of (6) leads to an important result. The expression K_i may be eliminated from $(6)_{1,2,3}$ to produce the well-known universal relations of [8], *viz.*,

$$
\frac{\parallel K + \mu/3 \parallel}{\parallel K - 2\mu/3 \parallel} = \frac{k_i^* - K_v - \mu_v/3}{l_i^* - K_v + 2\mu_v/3} = \frac{l_i^* - K_v + 2\mu_v/3}{n_i^* - K_v - 4\mu_v/3}.
\tag{8}
$$

Thus the knowledge, say, by an independent method or otherwise, of one of the properties fixes the other two. The structure of (8) lead [1] to introduce two microstructural parameters A_k and A_m, having a simple physical interpretation, namely, they represent, respectively, the mean transverse

hydrostatic strain and mean deviatoric strain in the fiber phase per unit applied transverse pressure and shear to yield

$$A_k = 1 + \| K - \mu/3 \| K_i/\mu_1,$$
$$A_m = M_i. \tag{9}$$

Thus exact formulae is also obtained for A_k and A_m.

3.1. Empty fibers

The case of empty fibers is of interest for poroelasticity theory and their applications. See, for instance, a recent survey article on bone poroelasticity [4]. From (6) and (7), closed-form expressions can be derived in the limit, when the fiber properties tend to zero. The final formulae are

$$\begin{aligned} k_e^* &= (K_1 + \mu_1/3)V_1 - V_2(K_1 + \mu_1/3)^2 K_e/\mu_1, \\ l_e^* &= (K_1 - 2\mu_1/3)V_1 - V_2(K_1 + 2\mu_1/3)(K_1 - 2\mu_1/3)K_e/\mu_1, \\ n_e^* &= (K_1 + 3\mu_1/4)V_1 - V_2(K_1 - 3\mu_1/4)^2 K_e/\mu_1, \\ p_e^* &= \mu_1(1 - 2V_2 P_e), \\ m_e^* &= \mu_1(1 - 2V_2 M_e), \end{aligned} \tag{10}$$

where K_e, P_e and M_e can be obtained from (7) by substituting there the values of the parameters A_i, B_i, C_i, D_i, E_i, χ_i and κ_1, when the inclusion properties vanish. This has been shown in Appendix C. They are

$$\begin{aligned} -A_e = B_e = E_e = \chi = 1, \\ C_e = -2D_e = -1/G, \\ \kappa_1 = (K_1 + 7\mu_1/3)/(K_1 + \mu_1/3). \end{aligned} \tag{11}$$

The universal relation (8) also follows by setting $K_2 = \mu_2 = 0$, or from the elimination of K_e in $(10)_{1,2,3}$.

3.2. Rigid fibers

Expressions (6) and (7) also allow the consideration of another case of interest, that of rigid fibers. Results of this Subsection can be useful to investigate global behavior of nonlinear fibrous elastic composite, by applying the variational inequalities reported in [19]. An application to dielectric case will be shown in the next Section. Here the limit of very large values of the fiber properties is taken. The relevant remaining quantities become

$$\begin{aligned} k_r^* &= (K_1 + \mu_1/3)(1 + V_2 K_r), \\ p_r^* &= \mu_1(1 + 2V_2 P_r), \\ m_r^* &= \mu_1(1 + V_2 M_r), \end{aligned} \tag{12}$$

where K_r, P_r and M_r are given by

$$\begin{aligned} K_r &= 1 + \frac{\mu_1}{K_1 + \mu_1/3}[2G - (1 + \kappa_1)B_r \mathcal{V}_p^T \mathcal{M}_k^{-1} \tilde{\mathcal{V}}_p/V_1]/V_1, \\ P_r &= [1 - V_2 - \mathcal{V}_p^T \mathcal{M}_p^{-1} \tilde{\mathcal{V}}_p]^{-1}, \\ M_r &= (1 + \kappa_1^{-1})/[1 + R^2 H_r - \mathcal{V}_m^T \mathcal{M}_m^{-1} \tilde{\mathcal{V}}_m]. \end{aligned} \tag{13}$$

The parameters A_r, B_r, C_r, and χ_r in (12), (13), and in the infinite order vectors and matrices (see Appendix B), take the values

$$\begin{aligned} -A_r &= \chi_r = 1, \\ B_r &= -\kappa_1^{-1}, \\ C_r &= -2\mu_1/V_1(K_1 + 7\mu_1/3), \end{aligned} \tag{14}$$

whereas $H_1 = H$ is given by (B4), $G_r = G$ by $(A1)_7$ and κ_1 by $(A1)_9$.

Equations (14)–(15) are derived from (6) and (7) by calculating the limit as $(\mu_2, K_2) \to (\infty, \infty)$. In this case, the evaluation is not direct and requires of some intermediate steps that are illustrated in Appendix E. A summary of the limits of A_i, B_i, C_i and χ as $(\mu_2, K_2) \to (\infty, \infty)$ is given in Appendix D.

Note that

$$P_e^{-1} - P_r^{-1} = 2V_2. \tag{15}$$

4. Numerical examples

4.1. Two-phase elastic composite

The material properties, of the binary composite considered here, were taken from [20]. The epoxy matrix Young modulus is $E_1 = 3.45$ GPa and Poisson ratio is $\nu_1 = 0.35$; correspondingly, the glass fibers values are $E_2 = 73.1$ GPa and $\nu_2 = 0.22$. It is of interest to compare the exact results calculated using the asymptotic homogenization method (AHM) with upper and lower bounds of normalized material and engineering constants as a function of the fiber volumetric fraction V_2 up to the percolation limit, which is $V_2 = \pi/4\sin(\pi/3)$. This is shown in Fig. 2. The plane bulk modulus ratio k^*/K_1 and the plane rigidity ratio m_i^*/μ_1 are plotted in Figs. 2a and 2b, respectively. The AHM curve is shown as the continuous line; the upper (lower) bound is plotted as the dash-dotted (dotted) line. The axial and transverse Young modulus ratio E_a^*/E_1 and E_t^*/E_1, are displayed in Figs. 2c and 2d, respectively. In Figs. 2a, b, c, d, the typical stiffening behaviour of the reinforcing fiber is shown. The property becames stiffer as the volume fraction V_2 of the fiber increases. The axial and transverse Poisson's ratio normalized relative to the matrix value ν_a^*/ν_1 and ν_t^*/ν_1 appear in Figs. 2e and 2f, respectively. The bounds due to Hill and Hashin were taken from [3] for k^*, m^*, E_a^*, ν_a^* and from [7] for E_t^* and ν_t^*. It is found that the AHM solution always lies between the bounds. Two extreme cases are shown in Figs. 2c and 2f. In the former case the bounds lie on top of each other, as the exact solution. In the latter case, the exact solution is not close to the bounds. On the other hand, the exact solution and a bound are very close to each other; see Figs. 2a, b, d for closeness to the lower bound and Fig. 2e to the upper bound. This means that the simple formulae given by the bound approximates the exact solution very well in almost all the volume fraction interval.

As the next example, the plane dimensionless properties dependence on the ratio μ_2/μ_1 against volume fraction V_2 in Figs. 3a, b, c, d. The shear modulus ratio μ_2/μ_1 ranges over 0 (empty fiber; full dotted line), 0.9 (dashed), 20 (dash-dotted), 120 (dotted line) and ∞ (rigid fiber; continuous) for the ratios of the transverse bulk modulus k_i^*/K_1 in Fig. 3a, transverse shear modulus m_i^*/μ_1 in Fig. 3b, transverse Poisson's ratio ν_t^*/ν_1 in Fig. 3c, and, finally, transverse Young's modulus E_t^*/E_1 in Fig. 3d. A typical fanning behaviour of the curves (non-intersecting) with fixed ratio μ_2/μ_1 as fan ribs is shown in Figs. 3a, b, d. The empty and rigid cases bound all others. The curve corresponding to empty fibers is monotone decreasing, characteristic of a fiber-weakened composite. As the material in the fiber becomes stiffer, the composite becomes stiffer so as to reach the limiting rigid behaviour, which is monotone increasing. Note that the composite is weakened (reinforced) when $\mu_2/\mu_1 < 1 (> 1)$. A different behaviour is shown in Fig. 3c for ν_t^*/ν_1 as far as $\mu_2/\mu_1 > 1$;

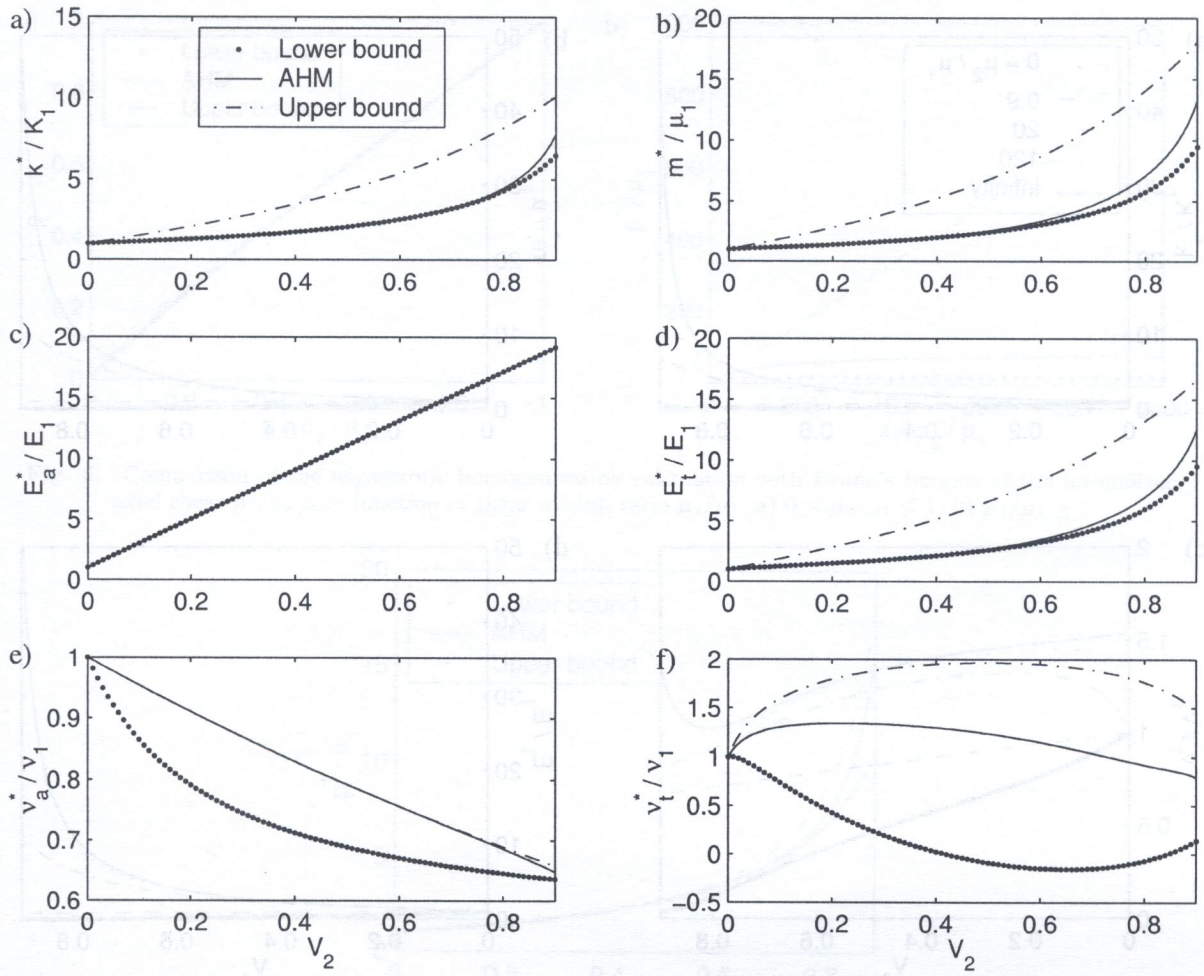

Fig. 2. For glass fibers in epoxy. Plots, versus fiber volume fraction V_2, of dimensionless effective plane a) bulk k_i^*/K_1, b) shear m_i^*/μ_1; c) axial E_a^*/E_1, d) transverse Young's E_t^*/E, moduli; normalized effective, e) axial ν_a^*/ν_1 and f) transverse Poisson's ratios ν_t^*/ν_1. Upper and lower bounds are shown as well as the calculated asymptotic homogenization solution

the curves are not longer monotone. Non-intersecting curves are obtained as well over the range of μ_2/μ_1 between 0 and ∞ the empty and rigid curves act as bounds again, the rigid curve does not start at $\nu_t^*/\nu_1 = 1$ for $V_2 = 0$, and display a somewhat different behaviour as compared with the rest of the curves.

The next example deals with the most fiber-weakened composite. The empty fiber one. The axial and transverse dimensionless engineering properties, Young's and shear moduli and Poisson's ratio, as a function of V_2, are shown in Figs. 4a, b, respectively. The dimensionless axial Poisson's ratio is constant over the whole interval and the dimensionless Young and shear moduli are monotone decreasing as displayed in Fig. 4a. Similar latter behaviour is followed by the dimensionless transverse Young and shear moduli and Poisson's ratio as can be seen in Fig. 4b.

The following example considers the normalized transverse shear modulus p^*/p_1 as a function of μ_2/μ_1. Figure 5a shows the case when $0 < \mu_2/\mu_1 < 1$ and Fig. 5b that when $\mu_2/\mu_1 > 1$ as the continuous line. Both figures also display Bruno's bounds taken from [2]. The computations were carried for the percolation limit $V_2 = \pi/4\sin(\pi/3)$ as an extreme case. The asymptotic homogenization solution lies between the bounds. For $0 < \mu_2/\mu_1 < 1$, the bounds are very sharp as can be seen in Fig. 5a. Not so for $\mu_2/\mu_1 > 1$ which tends to an almost constant value for large values of μ_2/μ_1.

Finally, the normalized transverse shear modulus p_i^*/p_1 is plotted against the fiber volume fraction (continuous line) in Fig. 6. The sharp bounds of Bruno are also shown. The computed value lies between the bounds.

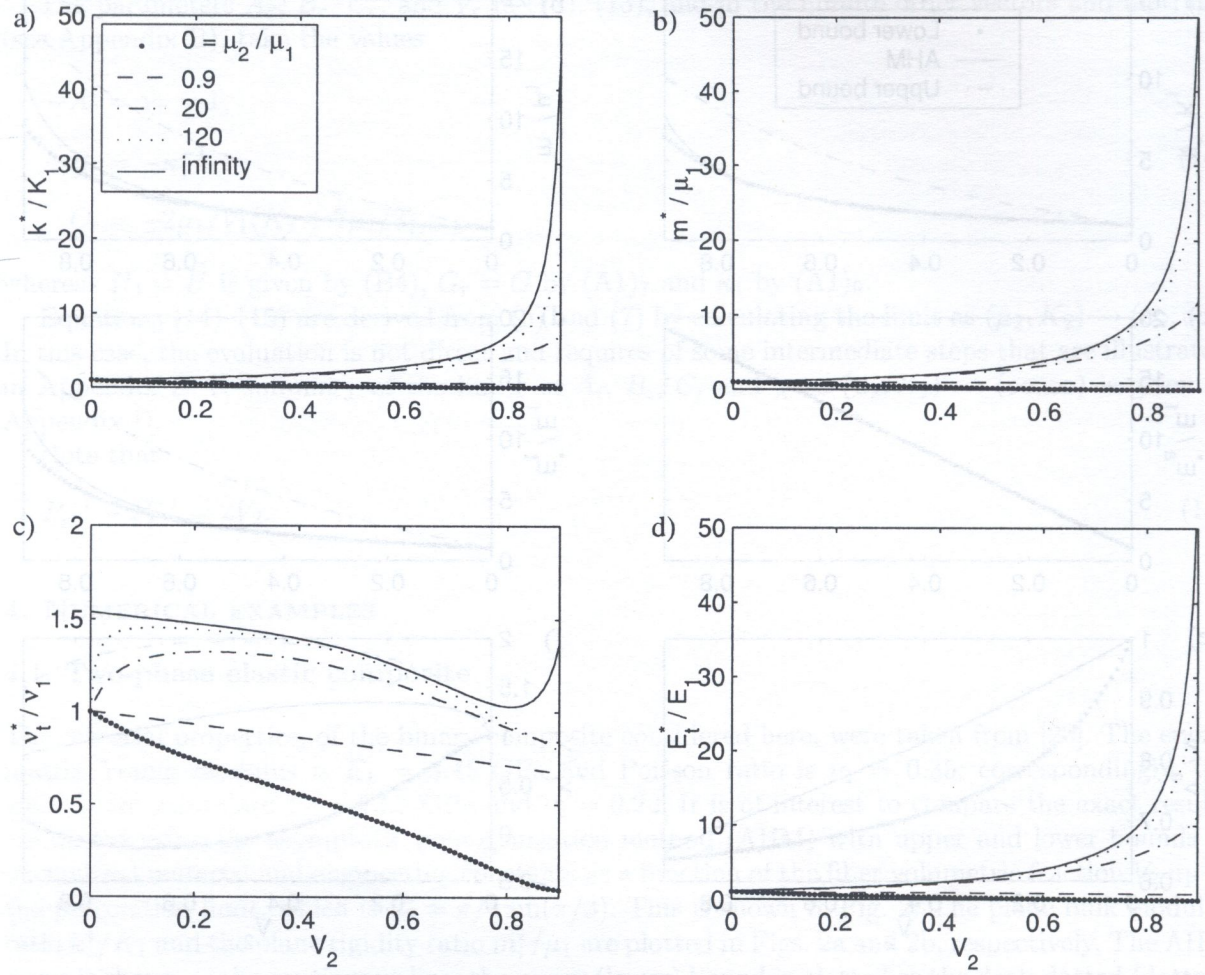

Fig. 3. The dependence of normalized effective parameters as a function of the ratio $\mu_2/\mu_1 = 0$ (empty), 0.9, 20, 120 and ∞ (rigid) of plane a) bulk k_i^*/K_1 and b) shear m_i^*/μ, moduli; transverse c) Poisson's ratio ν_t^*/ν_1 and d) Young's E_t^*/E_1 modulus. Note the bounding effect of empty and rigid fibers

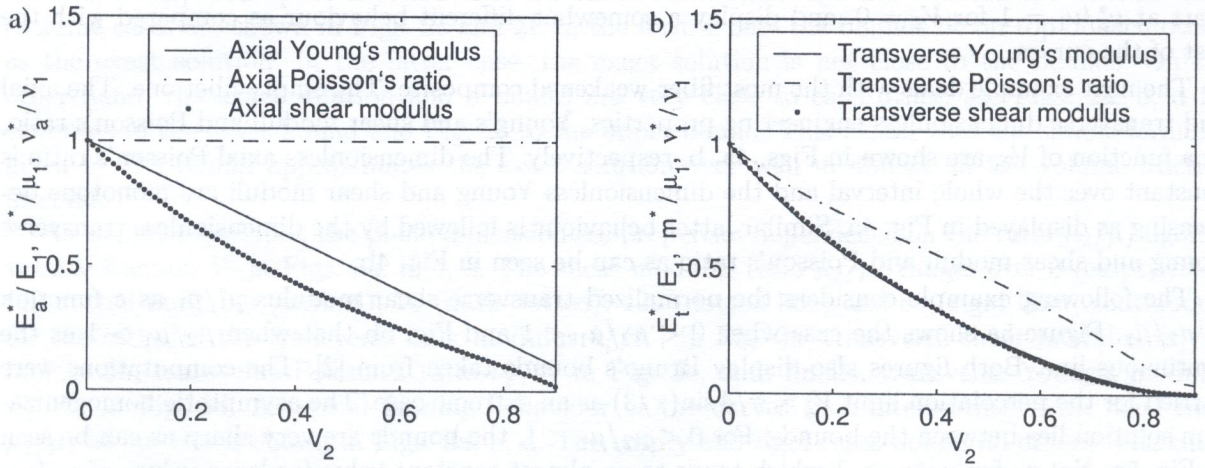

Fig. 4. Normalized effective property of empty fibers as a function of fiber volume fraction V_2 of a) axial Young's E_a^*/E_1, shear moduli p^*/E_1 and Poisson's ratio ν_a^*/ν_1; b) as (a) but for transverse properties: $E_t^*/E_1, m^*/\mu_1$ and ν_t^*/ν_1

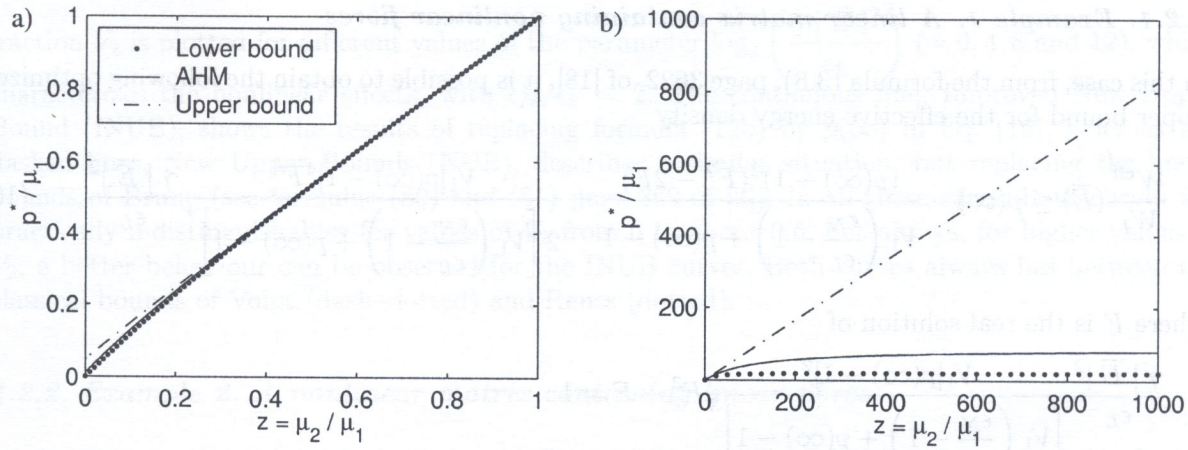

Fig. 5. Comparison of the asymptotic homogenization calculation with Bruno's bounds of the normalized axial shear p^*/μ_1 as a function of shear moduli ratio μ_2/μ_1. a) $0 \leq \mu_2/\mu_1 \leq 1$, b) $\mu_2/\mu_1 \geq 1$

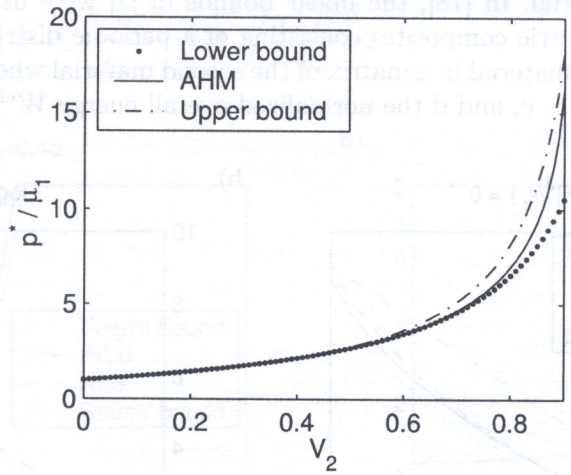

Fig. 6. Plot of the normalized effective axial shear modulus p^*/μ_1 as a function of fiber volume fraction V_2. Also the sharper Bruno bounds are plotted. This case also applies to the dielectric constant and is used for the calculations shown in Figs. 7 and 8

4.2. An application to nonlinear composites

This part is designed to show an application of above formulae for the effective properties to obtain bounds of the effective properties of nonlinear fibrous composites. The variational procedure described in [18], which incorporate microstructural information, is used here. This formulation uses a comparison material [17] and allows the construction of bounds for the overall energy of any composites whose material behavior is characterized by a convex potential function. Two examples of bounds for a matrix-fibre composite will be illustrated in the context of nonlinear electrostatics although these results also can be applied to nonlinear elastic composites as is demonstrated in [19]. These examples are related with the problem of bounding the effective energy density of a dielectric composite whose response is described by a convex potential function W^{eff}. Particularly, a two-phase fibrous composite consisting of one isotropic linear phase, with energy function

$$W_L(E) = \frac{1}{2}\epsilon_L \mid E \mid^2$$

and one isotropic nonlinear phase with energy function

$$W_N(E) = \frac{1}{2}\epsilon_N \mid E \mid^2 + \frac{1}{4}\gamma \mid E \mid^4,$$

where ϵ_L, ϵ_N and γ are constants and E is the electric field.

4.2.1. Example 1. A linear matrix containing nonlinear fibres

In this case, from the formula (3.8), page 3622, of [18], it is possible to obtain the following optimized upper bound for the effective energy density

$$\frac{W^{\text{eff}}}{W_L}(\overline{E}) \leq p(\infty) - \frac{(p(\infty)-1)^2(F^2-2F)}{V_1\left(\frac{\epsilon_N}{\epsilon_L}-1\right)+p(\infty)-1} + \frac{V_1[p(\infty)-1]^4F^4}{2\left[V_1\left(\frac{\epsilon_N}{\epsilon_L}-1\right)+p(\infty)-1\right]^4}\frac{\gamma\mid\overline{E}\mid^2}{\epsilon_L}, \tag{16}$$

where F is the real solution of

$$\frac{\gamma\mid\overline{E}\mid^2}{\epsilon_L}\frac{V_1[p(\infty)-1]^2}{\left[V_1\left(\frac{\epsilon_N}{\epsilon_L}-1\right)+p(\infty)-1\right]^3}F^3+F=1$$

and $\overline{E}$ is the mean value of E. Here, $p(\infty)$ is always an upper bound for the effective properties p of the comparison material. In [18], the linear bounds of [2] were used for obtaining improved bounds for nonlinear dielectric composites consisting of a periodic distribution of equal sized non-overlapping spheres of one material in a matrix of the second material where the inclusion phase does not percolate. In Figs. 7a, b, c, and d the normalized overall energy W^{eff}/W_L against fibre volume

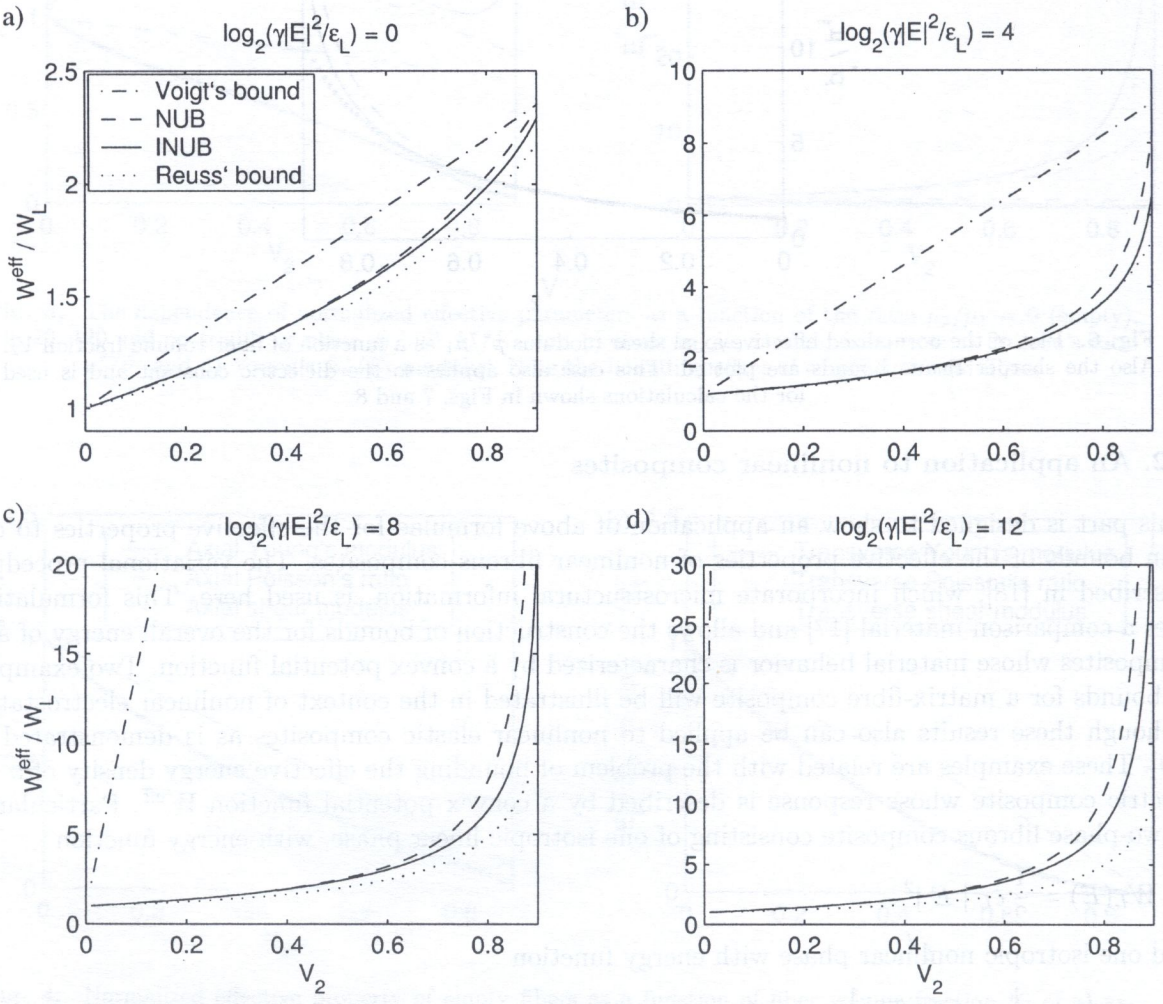

Fig. 7. Bounds for nonlinear fibers in a linear matrix. Plots of the normalized effective energy W^{eff}/W_L as a function of the fiber volume fraction V_2. The nonlinear parameter variation $\log_2(\gamma|\bar{E}|^2/\epsilon_L)$ takes the values $0, 4, 8, 12$ in (a), (b), (c), (d), respectively

fraction V_2 is plotted for different values of the parameter $\log_2\left(\frac{\gamma \mid \overline{E} \mid^2}{\epsilon_L}\right)$ $(= 0, 4, 8$ and $12)$, which characterizes the nonlinear effects, with $\epsilon_N/\epsilon_L = 2$. The continuous line, Improved New Upper Bound (INUB), shows the results of replacing formula (12b) by $p(\infty)$ in Eq. (16), whereas the dashed lines, New Upper Bounds (NUB), describes a similar situation, but replacing the linear bounds of Bruno (see formulae (80) and (81) page 369 of [2]). In all these cases, both curves are practically indistinguishables for values of V_2 from 0 to about 0.6, but always, for higher values of V_2, a better behaviour can be observed for the INUB curves. Both curves always lies between the classical bounds of Voigt (dash–dotted) and Reuss (dotted).

4.2.2. Example 2. A nonlinear matrix containing linear fibres

In this case, by using formula (3.9), page 3622, of [18] the following lower bound for the effective energy density can be derived

$$\frac{W^{\text{eff}}}{W_L}(\overline{E}) \geq \frac{\epsilon_o}{\epsilon_L} p_i \left(\frac{\epsilon_L}{\epsilon_o}\right) + V_2 \left(\frac{\epsilon_N}{\epsilon_L} - \frac{\epsilon_o}{\epsilon_L}\right)^2 \Big/ \frac{\gamma \mid \overline{E} \mid^2}{\epsilon_L}, \tag{17}$$

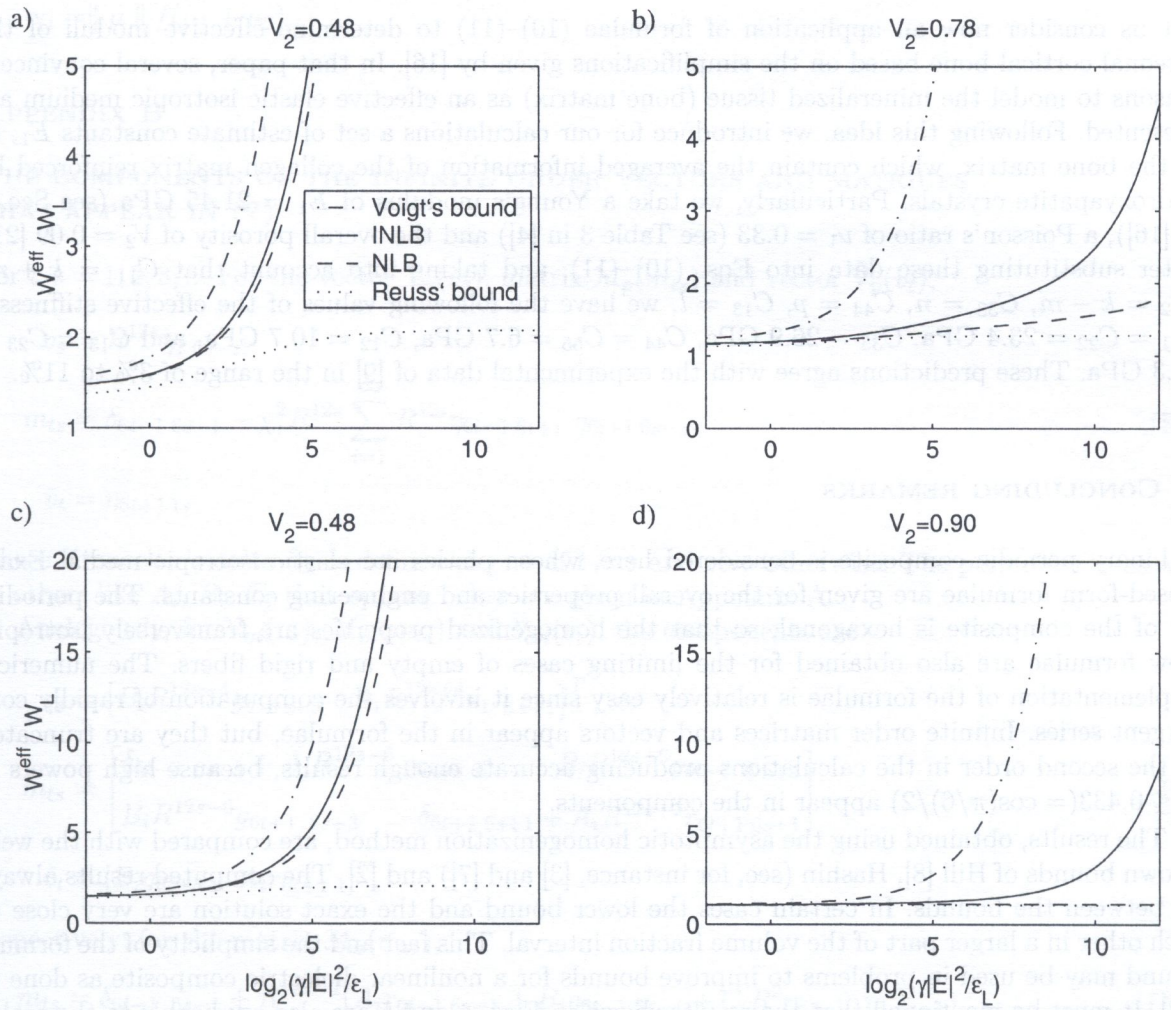

Fig. 8. Bounds for linear fibers in a nonlinear matrix for a square array (a), (b) and a hexagonal one (c), (d). Plots of the normalized energy W^{eff}/W_L as a function of the nonlinear parameter as $\log_2(\gamma|E|^2/\epsilon_L)$. The fiber volume fraction V_2 takes the values 0.48 and 0.78 in (a) and (b) respectively and 0.48 and 0.90 in (c) and (d), in that order

where ϵ_o is a free parameter. Any lower bound for the effective property $p_i(z)$, $z = \epsilon_L/\epsilon_0$, can be used in (17) and the best bound follows by maximizing the right-hand side of (17) with respect to ϵ_o. In Figs. 8a, b, c and d the normalized effective energy W^{eff}/W_L against the parameter $\log_2\left(\dfrac{\gamma \mid \overline{E} \mid^2}{\epsilon_L}\right)$ is plotted for differents values of V_2 and for $\epsilon_N/\epsilon_L = 2$. Here the curves appearing in Figs. 8a and 8b (for $V_2 = 0.48$ and 0.78) were computed for two-phase fibrous composites with a cell of periodicity of square type. The other Figs. 8c and 8d (for $V_2 = 0.48$ and 0.90) shows curves which corresponds to that of a hexagonal arrangement. As in Fig. 7 of Example 1, the dashed lines are computed replacing $p_i(z)$ with the linear bounds of [2] in Eq. (17). The continuous lines in Figs. 8c and 8d are also obtained from Eq. (17), but replacing $p_i(z)$ by the formula (3.1d) of [15]. It can be noted that in all cases the continuous line is over the dashed line in almost all the interval of variation of the parameter $\log_2\left(\dfrac{\gamma \mid \overline{E} \mid^2}{\epsilon_L}\right)$. In Figs. 8b and 8d the comparison is shown near the percolation value $V_2 = \pi/4$ and $V_2 = \pi/4\sin(\pi/3)$ respectively, where the improvement of the INLB curves respect to the NLB curves is remarkable. Other complementary results can be found in [12].

4.2.3. An application to bone mechanics

Let us consider now an application of formulae (10)–(11) to determine effective moduli of the osteonal cortical bone based on the simplifications given by [16]. In that paper, several convincent reasons to model the mineralized tissue (bone matrix) as an effective elastic isotropic medium are presented. Following this idea, we introduce for our calculations a set of estimate constants E_1, ν_1 of the bone matrix, which contain the averaged information of the collagen matrix reinforced by hydroxyapatite crystals. Particularly, we take a Young's modulus of $E_1 = 21.45$ GPa (see Sec. 3 in [16]), a Poisson's ratio of $\nu_1 = 0.33$ (see Table 3 in [4]) and the overall porosity of $V_2 = 0.09$ [21]. After substituting these data into Eqs. (10)–(11), and taking into account that $C_{11} = k + m$, $C_{12} = k - m$, $C_{33} = n$, $C_{44} = p$, $C_{13} = l$, we have the following values of the effective stiffnesses $C_{11} = C_{22} = 23.4$ GPa, $C_{33} = 26.9$ GPa, $C_{44} = C_{55} = 6.7$ GPa, $C_{12} = 10.7$ GPa, and $C_{13} = C_{23} = 11.3$ GPa. These predictions agree with the experimental data of [9] in the range of 3% to 11%.

5. Concluding remarks

A binary periodic composite is considered here, whose phases are elastic isotropic media. Exact closed-form formulae are given for the overall properties and engineering constants. The periodicity of the composite is hexagonal, so that the homogenized properties are transversely isotropic. New formulae are also obtained for the limiting cases of empty and rigid fibers. The numerical implementation of the formulae is relatively easy since it involves the computation of rapidly convergent series. Infinite order matrices and vectors appear in the formulae, but they are truncated to the second order in the calculations producing accurate enough results, because high powers of $R \leq 0.433 (= \cos(\pi/6)/2)$ appear in the components.

The results, obtained using the asymptotic homogenization method, are compared with the well-known bounds of Hill [8], Hashin (see, for instance, [3] and [7]) and [2]. The computed results always lie between the bounds. In certain cases the lower bound and the exact solution are very close to each other in a larger part of the volume fraction interval. This fact and the simplicity of the formula bound may be used in problems to improve bounds for a nonlinear dielectric composite as done in [18]. It must be mentioned that the results shown in Figs. 4 and 5 are also applicable to the scalar dielectric problem, in Figs. 6 and 7, because the formulae for the transverse shear modulus uncouples from the rest of the parameters. The exact formulae (6), (10), (12) and the universal relations (8) may be useful for checking numerical codes and experimental data.

Appendix A

Parameters that enter into equations (7) and (B1)–(B4)

$$
\begin{aligned}
A_i &= (\kappa_1\chi_\mu - \kappa_2)B_i/(\kappa_2 + \chi_\mu),\\
B_i &= (1-\chi_\mu)/(1+\kappa_1\chi_\mu),\\
C_i &= [(\kappa_1-1)\chi_\mu - (\kappa_2-1)]\,B_i/F_i,\\
D_i &= (\kappa_2-1)B_i/2F_i,\\
E_i &= B_i/(1-\chi_\mu),\\
F_i &= V_1\chi_\mu + (\kappa_2-1)G_i,\\
G_i &= 1/2 + V_2/(\kappa_1-1),\\
\chi_\mu &= \mu_2/\mu_1,\\
\kappa_j &= (K_j + 7\mu_j/3)/(K_j + \mu_j/3), j = 1,2,\\
\chi_i &= \| \mu \| /(\mu_1+\mu_2).
\end{aligned}
\tag{A1}
$$

Appendix B

The components of the infinite order vectors and matrices that appear in (7)

For $t, s = 1, 2, 3, \ldots$ For the vector $\mathcal{V}_p(v_s)$, matrix $\mathcal{M}_p(m_{ts})$ and vector $\tilde{\mathcal{V}}_p(v_t)$,

$$
\begin{aligned}
v_s &= R^{12s}\eta_{1\ 6s-1},\\
m_{ts} &= \delta_{6t-1\ 6s-1} - \chi_i^2 R^{12s}\sum_{i=1}^{\infty} R^{12i}\eta_{6t-1\ 6i+1}\,\eta_{6i+1\ 6s-1},\\
\tilde{v}_t &= \eta_{6t+1\ 1},
\end{aligned}
\tag{B1}
$$

where Kronecker's delta δ_{ts} is defined as one, if $t = s$ and zero otherwise. The parameter χ as well as others like A_i, B_i, C_i that appear below are given in Appendix A.

Analogously, for $\mathcal{V}_m(v_s)$, $\mathcal{M}_m(m_{ts})$ and $\tilde{\mathcal{V}}_m(v_t)$, the components are

$$
\begin{aligned}
v_s &= \left[B_i R^{12s-4} g_{1\ 6s-3} \quad A_i R^{12s+4} r_{1\ 6s+1}\right]^T,\\
m_{ts} &= \begin{bmatrix} \delta_{6t-3\ 6s-3} + A_i R^{12s-6}\, r_{6t-3\ 6s-3} & B_i R^{12s+6} g_{6t-1\ 6s+1} \\ B_i R^{12s-6} g_{6t+1\ 6s-3} & \delta_{6t+1\ 6s+1} + A_i R^{12s+2} r_{6t+1\ 6s+1} \end{bmatrix},\\
\tilde{v}_t &= [B_i g_{6t-3\ 1} \quad A_i r_{6t+1\ 1}]^T,
\end{aligned}
\tag{B2}
$$

respectively; for the matrix $\mathcal{M}_k(m_{ts})$,

$$
m_{ts} = \delta_{6t-1\ 6s-1} + R^{12s-2}(A_i r_{6t-1\ 6s-1} + B_i g_{6t-1\ 6s-1} + C_i R^2 \eta_{6t-1\ 1}\eta_{1\ 6s-1}).
\tag{B3}
$$

Also

$$
H_i = A_i r_{1\ 1} + \pi\kappa_1 B_i/\sin(\pi/3).
\tag{B4}
$$

Certain rapidly convergent series related to doubly elliptic functions of periods $\omega_1 = 1$ and $\omega_2 = e^{i\pi/3}$, which appear in (B1)–(B3), are given as follows:

$$\begin{aligned} S_{k+l} &= \sum_{m,n}{}' \beta_{mn}^{-k-l} \quad \text{for} \quad k+l \geq 3, \\ T_{k+l} &= \sum_{m,n}{}' \bar{\beta}_{mn} \beta_{mn}^{-k-l-1} \quad \text{for} \quad k+l \geq 3, \\ \eta_{kl} &= -C_{k+l-1}^{l} S_{k+l}, \\ \eta'_{kl} &= C_{k+l}^{l} T_{k+l}, \end{aligned} \tag{B5}$$

where $\beta_{mn} = m\omega_1 + n\omega_2$ for $m, n = 0, 1, 2, ...$; that the term $m = n = 0$ is excluded from the summation is indicated by the prime on the sigma symbol and $C_k^l = k!/l!(k-l)!$ Note that $S_2 \equiv T_2 \equiv 0$ by definition.

As well

$$\begin{aligned} r_{kl} &= \sum_{i=3}^{\infty}{}^{o} R^2 \eta_{ki} \eta_{il}, \\ g_{kl} &= k\left(\frac{k+l+2}{l+1} R^2 \eta_{k+2\,l} + \eta'_{kl}\right), \end{aligned} \tag{B6}$$

for $k, l = 1, 3, 5, ...$ The superindex o next to the summation symbol means that the sum is over odd indices only. The double series $\sum_{k,l} r_{kl}$, $\sum_{k,l} g_{kl}$ and $\sum_{k,l} \eta_{ki}\eta_{l1}$ are absolutely convergent. The above series are quickly convergent.

Appendix C

Limit of parameters A_i, B_i, C_i, D_i, E_i and χ_i as $(\mu_2, K_2) \to (0, 0)$

If the material properties of the matrix, μ_1 and K_1, and the volume fractions, V_1 and V_2, are fixed, then the parameters B_i, C_i, D_i, E_i and χ_i (see Appendix A) are functions of only one variable (μ_2 or K_2) and their limits can be directly calculated by using known theorems of classical mathematics analysis.

After previous algebraic transformations, taken from $(A1)_{2,3,4,5}$ and $(A1)_{10}$, the following results can be obtain

$$B_i = \frac{\mu_1 - \mu_2}{\mu_1 + \kappa_1 \mu_2} \to 1, \tag{C1}$$

$$C_i = \frac{[(\kappa_1 - 1)K_2 - 2\mu_1]B_i}{V_1 K_2 + 2\mu_1 G_i} \to \frac{-1}{G_i}, \tag{C2}$$

$$D_i = \frac{\mu_1 B_i}{V_1 K_2 + 2\mu_1 G_i} \to \frac{1}{2G_i}, \tag{C3}$$

$$E_i = \frac{B_i}{1 - \mu_2/\mu_1} \to 1, \tag{C4}$$

$$\chi = \frac{\mu_1 - \mu_2}{\mu_1 + \mu_2} \to 1. \tag{C5}$$

Under above conditions, the parameter A_i is a function of two variables μ_2 and K_2 and can be expressed as follows

$$A_i = \frac{\kappa_1\mu_2K_2 - \mu_1K_2 - 2\mu_1\mu_2}{\mu_2K_2 + \mu_1K_2 + 2\mu_1\mu_2} \cdot B_i. \tag{C6}$$

As we can note, from (C6), the iterative limits $\lim_{\mu\to 0}\lim_{K_2\to 0} A_i = \lim_{K_2\to 0}\lim_{\mu_2\to 0} A_i = -1$ and, therefore, it is natural to intent to prove that

$$A_i \to -1 \tag{C7}$$

as $(\mu_2, K_2) \to (0,0)$. In fact, it is possible to verify that

$$\left|\frac{A_i}{B_i} + 1\right| = \left|\frac{(\kappa_1 + 1)\mu_2K_2}{\mu_2K_2 + \mu_1K_2 + 2\mu_1\mu_2}\right|. \tag{C8}$$

By substituting $\mu_2 = \rho\cos\theta$, $K_2 = \rho\sin\theta$ (ρ, θ polar coordinates) into (C8), and by simplifying we have

$$\left|\frac{A_i}{B_i} + 1\right| = \left|\frac{(\kappa_1 + 1)\rho\cos\theta\sin\theta}{\mu_1(\sin\theta + \cos\theta) + \rho\cos\theta\sin\theta}\right| \to 0 \tag{C9}$$

as $\rho \to 0$.

Appendix D

Limit of parameters A_i, B_i, C_i and χ_i as $(\mu_2, K_2) \to (\infty, \infty)$

As in Appendix C, for fixed values of μ_1, K_1, V_1 and V_2 the following limits can be derived by direct evaluation

$$B_i = \frac{\mu_1 - \mu_2}{\mu_1 + \kappa_1\mu_2} \to -\frac{1}{\kappa_1}, \tag{D1}$$

$$C_i = \frac{[(\kappa_1 - 1)K_2 - 2\mu_1]B_i}{V_1K_2 + 2\mu_1G_i} \to \frac{1 - \kappa_1}{\kappa_1V_1}, \tag{D2}$$

$$\chi = \frac{\mu_1 - \mu_2}{\mu_1 + \mu_2} \to -1. \tag{D3}$$

Whereas, as will be shown inmediately, for parameter A_i results

$$A_i \to -1. \tag{D4}$$

In fact, by introducing the polar coordinates $\mu_2 = \rho\cos\theta, K_2 = \rho\sin\theta$ into Eq. (C6), and after some algebraic manipulations, we have

$$|B_i\kappa_1 - A_i| = |B_i| \cdot \left|\frac{\kappa_1\mu_1\sin\theta + 2\kappa_2\mu_1\cos\theta + \mu_1\sin\theta + 2\mu_1\cos\theta}{\rho\cos\theta\sin\theta + \mu_1\sin\theta + 2\mu_1\cos\theta}\right|$$

and, consequently $|B_i\kappa_1 - A_i| \to 0$ as $\rho \to \infty$.

Appendix E

Derivation of formulae (12). Rigid fibers

a) Derivation of $(12)_1$

In order to solve the indeterminate forms involved in the calculation of the limit of K_i^* as $(\mu_2, K_2) \to (\infty, \infty)$, we may write $(6)_1$ as follows

$$K_i^* = (K_1 + \mu_1/3)V_1 + \alpha_i + \beta_i \tag{E1}$$

where

$$\begin{aligned} \alpha_i &= (K_2 + \mu_2/3)V_2 - \frac{V_1 V_2}{\mu_1}(K_1 + \mu_1/3 - K_2 - \mu_2/3)^2 \frac{D}{B}, \\ \beta_i &= \frac{\mathcal{V}_2(1+\kappa_1)}{\mu_1}\mathcal{V}_p^T \mathcal{M}_k^{-1}\tilde{\mathcal{V}}_p(K_1 + \mu_1/3 - K_2 - \mu_2/3)^2 \frac{D_1^2}{B_i}. \end{aligned} \tag{E2}$$

The functions α_i and β_i have $\mathcal{V}_P^T$ finite limit as $(\mu_2, K_2) \to (\infty, \infty)$. In fact, by substituting $(A1)_2$ and $(A1)_3$ into Eqs. (E2), and simplifying, we get

$$\begin{aligned} \alpha_i &= \frac{2V_2[G_i + \frac{V_1}{\mu_1}(K_1 + \mu_1/3)](K_2 + \mu_2/3) - \frac{V_1}{\mu_1}(K_1 + \mu_1/3)^2}{\frac{V_1}{\mu_1}(K_2 + \mu_2/3) + 2G_i} \\ \beta_i &= \frac{V_2(1+\kappa_1)\mathcal{V}_P^T \mathcal{M}_k^{-1}\tilde{\mathcal{V}}_P(K_1 + \mu_1/3 - K_2 - \mu_2/3)^2 B_i \mu_1}{[V_1(K_2 + \mu_2/3) + 2\mu_1 G_i]^2} \end{aligned} \tag{E3}$$

From equations (E3), as $(\mu_2, K_2) \to (\infty, \infty)$, results

$$\begin{aligned} \alpha_i &\to \frac{2V_2}{V_1}[G_i\mu_1 + (K_1 + \mu_1/3)V_1] \\ \beta_i &\to -\frac{V_2(1+\kappa_1)\mu_1 V_p^T \mathcal{M}_K^{-1}\tilde{V}_p}{V_1^2 \kappa_1} \end{aligned} \tag{E4}$$

By combining (E4) and (E1), the rigid effective coefficient K_r^* takes the form

$$K_r^* = (K_1 + \mu_1/3)V_1 + \frac{2V_2}{V_1}\Big[G_i\mu_1 + (K_1 + \mu_1/3)V_1\Big] + \frac{V_2(1+\kappa_1)\mu_1 \mathcal{V}_p^T \mathcal{M}_K^{-1}\tilde{\mathcal{V}}_p}{\mathcal{V}_1^2 \kappa_1} \tag{E5}$$

Finally, form (E5), collecting the term $K_1 + \mu_1/3$, using $V_1 + V_2 = 1$, and by transforming conveniently, the formulae $(12)_1$ and $(13)_1$ can be obtained.

b) Derivation of $(12)_2$

From $(6)_4$ and $(7)_2$, using $(A1)_{10}$, we have

$$p_i^* = \mu_1(1 - 2V_2\,\chi_i\,P_i) \tag{E6}$$

where

$$P_i = \frac{1}{1 + \chi_i V_2 - \chi_i^2 \mathcal{V}_p^T \mathcal{M}_p^{-1}\tilde{\mathcal{V}}_p} \tag{E7}$$

Taking limit as $\mu_2 \to \infty$ on both sides of (E6) and (E7), and using (D3), the effective formulae $(13)_2$ and $(13)_2$ can be derived.

c) Derivation of $(12)_3$

From $(6)_5$ and $(7)_3$ we have

$$m_i^* = \mu_1 - V_2(\mu_1 - \mu_2)(1+\kappa_1)E_i/(1 + R^2H_i - \mathcal{V}_m^T\,\mathcal{M}_m^{-1}\tilde{\mathcal{V}}_m). \tag{E8}$$

By substituting $(A1)_5$ into (E6), and by using $(A1)_8$ we can obtain

$$m^* = \mu_1 + \frac{V_2(1+\kappa_1)\mu_1 B_i}{(1 + R^2H - \mathcal{V}_m^T\mathcal{M}_m^{-1}\tilde{\mathcal{V}}_m)}. \tag{E9}$$

Taking into account (C1)–(C4) and (C7), evaluating in (E9) the limit as $(\mu_2, K_2) \to (\infty, \infty)$, collecting μ_1, and using $(13)_3$, one can get $(12)_3$.

Acknowledgments

This work was sponsored by PAPIIT, DGAPA, UNAM Project Number IN101705; DGI-MCT, ULL Proyect BFM2001-3894; project CITMA PNCIT IBMFQC 09-2004. Thanks are due to Ana Pérez Arteaga for computational support. The authors are grateful to D.R.S. Talbot for useful discussions and suggestions. J.B. would like to thank CIMAC Foundation for the award of one of its Fellowships.

References

[1] M. Avellaneda, P. J. Swart. Calculating the perfomance of 1–3 piezoelectric composites for hydrophone applications: an effective medium approach. *J. Acoust. Soc. Am.*, **103**: 1449–1467, 1998.

[2] O. Bruno. The effective conductivity of strongly heterogeneous composites. *Proc. R. Soc. Lond.*, **A 433**: 353–381, 1991.

[3] R. M. Christensen, *Mechanics of Composite Materials*. Krieger, Malabar, Fl., 1991.

[4] S. C. Cowin, Bone poroelasticity. *J. Biomechanics*, **32**: 217–238, 1999.

[5] E. I. Grigolyuk, L. A. Fil'shtinskii, *Perforated Plates and Shells* (in Russian). Nauka, Moscow, 1970.

[6] R. Guinovart-Díaz, R. Bravo-Castillero, J. Rodríguez-Ramos, F. J. Sabina. Closed-form expressions for the effective coefficients of fibre-reinforced composite with transversely isotropic constituents. I: Elastic and hexagonal symmetry. *J. Mech. Phys. Solids*, **49**: 1445–1462, 2001.

[7] Z. Hashin. Analysis of composite materials. A Survey. *J. Appl. Mech.*, **50**: 481–505, 1983.

[8] R. Hill. Theory of mechanical properties of fibre-strengthened materials: I. Elastic behavior. *J. Mech. Phys. Solids*, **12**: 199–212, 1964.

[9] J. L. Katz, H. S. Yoon, S. Lipson, R. Maharidge, A. Maunier, P. Christel. The effects of remodeling on the elastic properties of bone. *Calcified Tissue International*, **36**: 531–536, 1984.

[10] S. A. Meguid, A. L. Kalamkarov. Asymptotic homogenization of elastic composite materials with a regular structure. *Int. J. Solids Struc.*, **31**: 2933–2944, 1994.

[11] V. Z. Parton, B. A. Kudryavtsev, *Engineering Mechanics of Composite Structures*. CRC Press, Boca Raton, 1993.

[12] L. D. Pérez, A. León, J. Bravo-Castillero, Variational bounds for nonlinear fibrous composites. [In:] P. Kittl, G. Díaz, D. Mook, J. Geer, eds. Proc. Seventh Panamerican Congress of Applied Mechanics (PACAM VII), 105–108, 2002.

[13] B. E. Pobedrya. *Mechanics of Composite Materials* (in Russian). Moscow State University, Moscow, 1984.

[14] F. J. Sabina, R. Rodríguez-Ramos, J. Bravo-Castillero, R. Guinovart-Díaz. Closed-form expressions for the effective coefficients of fibre-reinforced composite with transversely isotropic constituents. I: Piezoelectric and hexagonal symmetry. *J. Mech. Phys. Solids*, **49**: 1463–1479, 2001.

[15] F. J. Sabina, J. Bravo-Castillero, Guinovart-Díaz, R. Rodríguez-Ramos, O. C. Valdiviezo-Mijangos. Overall behavior of two-dimensional periodic composites. *Int. J. Solids Struc.*, **39**: 483–497, 2002.

[16] I. Sevostianov, M. Kachanov. Impact of the porous microstructure on the overall elastic properties of the osteonal cortical bone. *J. Biomech.*, **33**: 881–888, 2000.

[17] D. R. S. Talbot, J. R. Willis. Some simple explicit bounds for the overall behavior of nonlinear composites. *Int. J. Solids Struc.*, **29**: 1981–1987, 1992.

[18] D. R. S. Talbot. Bounds which incorporate morphological information for nonlinear composite dielectric. *Proc. R. Soc. Lond.*, **A 455**: 3617–3628, 1999.

[19] D. R. S. Talbot. Improved bounds for the effective properties of a nonlinear two-phase elastic composite. *J. Mech. Phys. Solids*, **48**: 1285–1294, 2000.

[20] S. W. Tsai, H. T. Hahn. *Introduction to Composite Materials*. Technomic, Westport, 1980.

[21] D. Zhang, S. Weinbaum, S. C. Cowin, Estimates of the peak pressures in the bone pore water. *J. Biomech. Eng.*, **120**: 697–703, 1998.